

THERMAL BEHAVIOR OF DOUBLE ARC GROOVE FRICTION PAIRS IN HYDRO-VISCOUS DRIVE UNDER SOFT START-UP CONDITION

by

Qiliang WANG^a, Hongwei CUI^{a,b*}, Zisheng LIAN^{a,b}, and Long LI^a

^aCollege of Mechanical Engineering, Taiyuan University of Technology, Taiyuan, China

^bShanxi Key Laboratory of Fully Mechanized Coal Mining Equipment,
Taiyuan University of Technology, Taiyuan, China

Original scientific paper
<https://doi.org/10.2298/TSCI171111010W>

The 3-D transient heat conduction equations with boundary-value problems were established for numerical simulation to explore the thermal behavior of double arc groove friction pairs. The heat flux of the contact face decelerated with time, and its distributions were formulated with intensity proportional to the thermal parameters of the materials. Additionally, the theoretical expression of the friction disc's speed was deduced. Subsequently, a numerical solution was obtained using the finite difference method to predict the temperature field distributions of the friction pairs and to determine the location of the maximum temperature under different start-up times. The results indicate that the friction disc and steel disc are approximately similar regarding the temperature field distributions. However, the temperature and radial temperature gradient of the latter are several times those of the former. The temperature of the central region for each rhombus at the surface of the friction disc are higher than those of the surrounding area. The longer the time to soft start-up is, the higher is the generated temperature, and the greater is the radial temperature gradient. The analysis provides theoretical reference and technical support for the selection of the start-up time by considering the actual working conditions of scraper conveyor.

Key words: hydro-viscous drive, double arc groove, thermal behavior, transient temperature field, soft start-up process

Introduction

The hydro-viscous drive (HVD) uses viscous fluid as its working medium to transfer power, and relies on the fluid shear force and frictional force between the driving and driven discs, which is a new type of power transmission device. The HVD is mainly used for fans, water pumps, belt conveyors, scraper conveyors, and other mechanical equipment, and has the advantages of step-less speed regulation, soft start-up, overload protection, small start-up impact, high efficiency, and high reliability. Thereby, it realizes energy saving by reducing the energy consumption of the equipment [1].

In the process of soft start-up, a large amount of frictional heat is produced by the relative sliding between the driving and driven discs. This results in a sharp increase in the temperature of the discs. On the one hand, there is a strong thermal convection between the friction pairs and oil film, and a constant change in boundary conditions, which cause the non-uniform

* Corresponding author, e-mail: cuihongwei@tyut.edu.cn

distribution of the temperature field. On the other hand, large thermal stresses generated by high temperature may cause the deformation of friction pairs. Moreover, it has also been found that high thermal stresses occur in the friction pairs owing to the considerable temperature difference during the start-up process. Therefore, the distribution characteristics of the friction pairs' temperature field have been widely discussed.

There is an abundance of archival research publications dealing with thermal problems. A literature review was carried out regarding the numerical analysis of thermal stresses in disc brakes and clutches [2]. The analysis, of uncoupled and coupled thermoelasticity problem for frictional heat generation in disc brakes and clutches was carried using the finite element method. Zagrodzki and Truncone [3] found that severe hot spots can be produced during short-term clutch operation with a high initial sliding speed. Marklund and Larsson [4] and Marklund *et al.* [5] investigated the friction of a small wet clutch friction disc sample and obtained results that were in good agreement with the friction behaviors of different measurement methods. Hu, *et al.* [6] developed a uniform cross-speed model covering the average flow model and cavitation model, and studied the cross-speed characteristics of an end-face seal ring with spiral grooves for wet clutch. Addressed to serious heat degradation problem of the braking continuously performed in the drag brake application for a long time, finite element analysis for bi-directional thermal-structure coupling was performed to investigate the temperature and stress in the case where the material properties depend on temperature [7]. A series of finite element method investigations were carried out on the non-axisymmetric heating of the disc by the heat flux moving with the intensity proportional to the specific power of friction within a contact area, at a constant coefficient of friction [8-10].

Cui [11] and Cui, *et al.* [12] analyzed the influence of double arc oil groove parameters on shear torque by means of theory and experiment. Xie *et al.* [13] studied the influence of the different cross-sectional shapes and layout forms of oil grooves on thermal behavior, and determined the optimal section shape and layout form of oil grooves on the temperature field. Cui, *et al.* [14] established a 3-D transient temperature model to research the thermal behavior of multidisc friction pairs in HVD. An analysis was performed on the 3-D transient temperature field of a disc brake generated during a single and multiple braking processes with temperature dependent and constant coefficients of friction [15]. The thermal effects in the structure and contact behavior of a disc-pad assembly were identified by a finite element approach [16, 17]. Moreover, the structural and thermo-mechanical behavior of the dry contact between the brake disc and the pads during the braking phase were analyzed using the ANSYS simulation software [18, 19]. A FE model was proposed to determine the corresponding quasi-static stresses in the brake disc tribosystem [20].

In conclusion, the extant investigation only analyzed the thermal properties of the friction pairs under certain conditions. Additionally, the effect of the double arc groove on the distribution characteristics of the temperature field of the friction pairs has not been considered. In this study, the investigated friction pairs are used in a scraper conveyor, which has a long start-up time. The speed of the friction pairs is relatively low, however their radius is large. Since the actual working condition is very harsh, it is difficult to measure the temperature at various points when the friction pairs are at work. Therefore, the finite element method is a more desirable approach.

This study focused on the thermal characteristics of the double arc groove and obtained the temperature distribution for the friction pairs. Moreover, the location of the maximum temperature under different start-up times was predicted by establishing the 3-D transient heat conduction equations, deriving the theoretical expression of the friction disc's speed, and

determining the boundary conditions. These will be helpful in selecting of start-up time for the scraper conveyor.

Statement of the problem

Figure 1 illustrates the schematic of the HVD device, which uses a planet gear transmission mechanism. The internal ring gear is floating, the planet carrier is connected to the output shaft and the Sun gear rotates as the input shaft. The friction discs are attached to the internal ring gear by the external spline. The steel discs are attached to the fixed plate by the inner spline, and the fixed plate is attached to the shell steadily. The friction discs and steel discs shown in fig. 2 are arranged alternately along the axial direction, and lubricating oil is filled in the clearance between them. By controlling the pressure of the annular oil cylinder, the clearance between the friction pairs is adjusted. This realizes their bonding and separating for the speed and torque of the output shaft to be changed. Thereby, a soft start-up function is achieved. Owing to the constant static-state of the steel discs, the bonding of the friction pairs are realized by reducing the speed of the friction discs with planetary gear transmission during the entire soft start-up process.

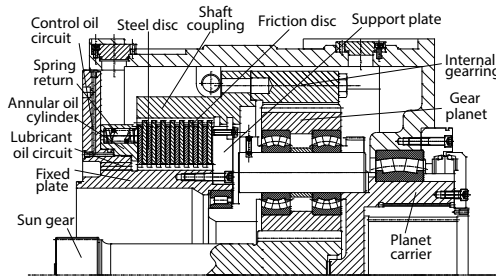


Figure 1. The schematic of the HVD device

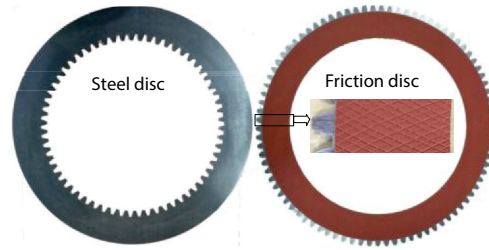


Figure 2. The picture of friction pairs

For the soft start-up of the scraper conveyor, the S-type start-up curve is the most ideal one, as shown in fig. 3. The entire start-up process is divided into three stages: no-load start of motor (0- t_1), pre-start of scraper conveyor (t_1 - t_3), and accelerated start of scraper conveyor (t_3 - t_4). The speed of the output shaft with time is given:

$$n_j(t) = \begin{cases} 0 & 0 \leq t < t_1 \\ \frac{t-t_1}{t_2-t_1} n_1 & t_1 \leq t < t_2 \\ n_1 & t_2 \leq t < t_3 \\ n_1 + \frac{n_0-n_1}{t_4-t_3} (t-t_3) - \frac{n_0-n_1}{2\pi} \sin \left[\frac{2\pi}{t_4-t_3} (t-t_3) \right] & t_3 \leq t \leq t_4 \end{cases} \quad (1)$$

where $t_1 = t_4/10$, $t_2 = t_1 + 2$, and $t_3 = t_4/2$.

According to the principle of planetary gear transmission, the speed of the friction disc is given:

$$n_f = \frac{\gamma+1}{\gamma} n_j - \frac{1}{\gamma} n_s = \frac{27}{22} n_j - \frac{5}{22} n_s \quad (2)$$

where n_f , n_j , and n_s are the speed of the friction disc, output shaft, and Sun gear, respectively, $n_s = 243$ r/min, $n_0 = 45$ r/min, $n_1 = n_0/10 = 4.5$ r/min, and $\gamma = 4.4$

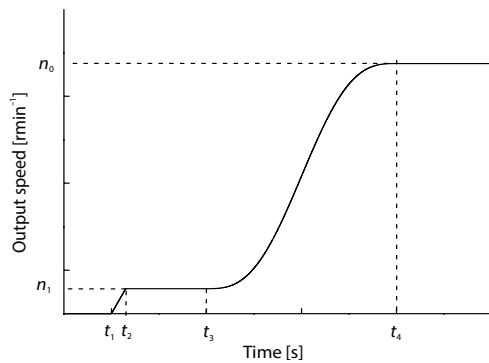


Figure 3. The start-up curve of the scraper conveyor

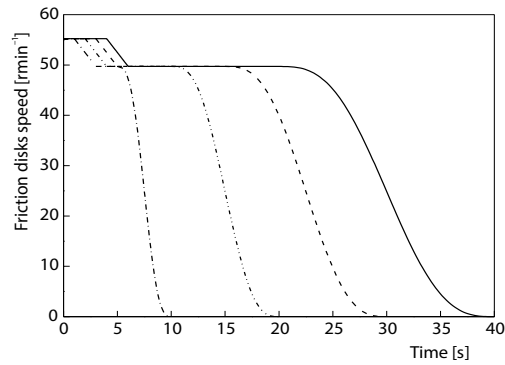


Figure 4. The speed of the friction disc under different start-up times

By substituting eq. (1) into (2), the speed of the friction disc can be obtained:

$$n_f = \begin{cases} \frac{5}{22} n_s & 0 \leq t < t_1 \\ \frac{5}{22} n_s - \frac{27}{22} \frac{t-t_1}{t_2-t_1} n_1 & t_1 \leq t < t_2 \\ \frac{5}{22} n_s - \frac{27}{22} n_1 & t_2 \leq t < t_3 \\ \left. \frac{5}{22} n_s - \frac{27}{22} \left[n_1 + \frac{n_0-n_1}{t_4-t_3} (t-t_3) - \frac{n_0-n_1}{2\pi} \sin \left[\frac{2\pi}{t_4-t_3} (t-t_3) \right] \right] \right\} & t_3 \leq t \leq t_4 \end{cases} \quad (3)$$

Therefore, in the entire start-up process, the speed of the friction disc follows an anti-S curve. Figure 4 shows the speed variation of the friction disc over time when the soft start-up time is 10, 20, 30, and 40 seconds, respectively.

Transient finite element analysis

The geometry and load of the friction disc and steel disc are symmetric about the mid-plane. During the start-up process, the gaps between the discs and oil flow are very small. Hence, the small part of the heat absorbed by the oil film is negligible. Moreover, the thermal property of isotropic materials does not vary with temperature. According to the previous analysis, some essential assumptions are made:

- the materials of the friction disc and steel disc are isotropic,
- the heat generated by friction is absorbed by the friction pairs entirely, and the radiative heat transfer from the disc is small enough to be negligible [8], and
- the computational region is restricted to half of their thickness.

By considering the axisymmetric structure of the friction pairs, the transient heat conduction differential equations for the friction pairs in cylindrical co-ordinates are given:

$$\rho_i c_i \frac{\partial T_i}{\partial t} = k_i \left(\frac{\partial^2 T_i}{\partial r^2} + \frac{1}{r} \frac{\partial T_i}{\partial r} + \frac{\partial^2 T_i}{\partial z_i^2} \right) \quad (4)$$

where the subscript i represents s, f, and c, which are the steel disc, friction lining, and core disc, respectively. The T_i , ρ_i , k_i , and c_i are the temperature, density, thermal conductivity, and specific heat of the material i , respectively.

The schematic of the overall heat exchange system is shown clearly in fig. 5. The friction surfaces CD and EF under the effect of frictional heat can be expressed as heat flux. The inner and outer surfaces AD, EH, BC, and FG of the discs are under the effect of heat convection. The middle surfaces AB and GH are adiabatic.

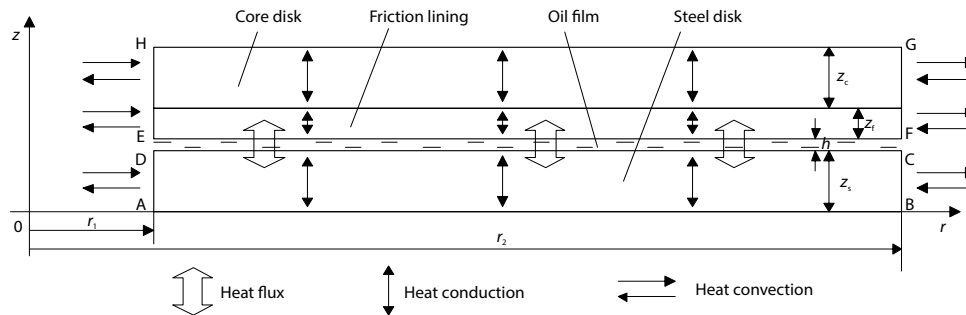


Figure 5. The schematic of the heat exchange system

Boundary conditions

Let us consider the steel disc as an example. The boundary conditions for the computation of the temperature are [14].

– Heat flux boundary condition:

$$k_s \frac{\partial T_s}{\partial z} \Big|_{z=z_s} = q_s(r, t), \quad r_1 \leq r \leq r_2, \quad 0 \leq t \leq t_4 \quad (5)$$

where q_s is the heat flux of the steel disc, which can be derived from the following model.

– Heat convection boundary conditions:

$$k_s \frac{\partial T_s}{\partial r} \Big|_{r=r_1} = \alpha_{s1} (T_a - T_s), \quad 0 \leq z \leq z_s, \quad t \geq 0 \quad (6)$$

$$k_s \frac{\partial T_s}{\partial r} \Big|_{r=r_2} = \alpha_{s2} (T_a - T_s), \quad 0 \leq z \leq z_s, \quad t \geq 0 \quad (7)$$

where α_{s1} and α_{s2} are, respectively, the convection coefficients on the inner and outer surfaces of the steel disc, and T_a is the ambient oil temperature.

– Initial temperature boundary condition:

$$T(r, z, t) \Big|_{t=0} = T_0, \quad r_1 \leq r \leq r_2, \quad 0 \leq z \leq z_s + h + z_f + z_c \quad (8)$$

where T_0 is the initial temperature of the steel disc.

– Adiabatic boundary condition:

$$\frac{\partial T_s}{\partial z} \Big|_{z=0} = 0, \quad r_1 \leq r \leq r_2, \quad t \geq 0 \quad (9)$$

Heat flux model and distribution coefficient

According to the principle of thermodynamics and the frictional power method, the heat flux of a friction surface is given by:

$$q(r, t) = \frac{4\mu Fr\omega(t)}{\pi(r_2^2 - r_1^2)} = \mu pr\omega(t) \quad (10)$$

where p and μ represent the normal pressure and frictional coefficient, respectively, ω is the relative angular velocity, $\omega = \omega_f = 2\pi n_f/60$, and r_1 and r_2 are the inner and outer radii of the discs, respectively.

According to eq. (10), the heat flux is related to the relative angular velocity and radius. The relative angular velocity changes with time, t , during the entire start-up process. Therefore, the temperature at a certain point of the friction pairs is related to time and the distance to the center.

$$q_s(r, t) = \lambda q(r, t) \quad (11)$$

$$q_f(r, t) = (1 - \lambda)q(r, t) \quad (12)$$

$$\lambda = \frac{\sqrt{\rho_s c_s k_s}}{\sqrt{\rho_s c_s k_s} + \sqrt{\rho_f c_f k_f}} \quad (13)$$

where λ is the distribution coefficient of the heat flux.

Solving the finite element model

The solution of the heat conduction problem is the numerical integration of eq. (4). The transient heat conduction differential equations were discretized using the Galerkin method to obtain the transient temperature field matrix:

$$[C]\{T'\} + [K]\{T\} = \{Q\} \quad (14)$$

where $[C]$ is the heat capacity matrix, $[K]$ – the heat conductivity matrix, $\{T\}$ – the node temperature vector, $\{T'\}$ – the time derivative of the node temperature vector, and $\{Q\}$ – the generalized node heat flux vector. The detailed derivation of eq. (14) can be found in [21].

The Newmark direct transient integral method is the most commonly used method for solving eq. (14). The assumed relationship between temperature T_n at time $t = t_n$, and temperature T_{n+1} at time $t = t_n + \Delta t$ is:

$$T_{n+1} = T_n + [(1 - \beta)T'_n + \beta T'_{n+1}] \Delta t \quad (15)$$

where β is a parameter that can be determined to obtain integration accuracy and stability. Stable schemes are usually obtained when β is in the range of $0.5 \leq \beta \leq 1.0$.

By substituting eq. (15) into eq. (14), we can obtain an implicit algebraic equation:

$$([C] + \beta \Delta t [K])T_{n+1} = ([C] - (1 - \beta)[K] \Delta t)T_n + (1 - \beta) \Delta t \{Q\}_n + \beta \Delta t \{Q\}_{n+1} \quad (16)$$

Equation (16) is a formula for solving the equation of the transient temperature field and can be used to obtain the temperature at any time. Therefore, this method can be regarded as an implicit finite difference method. In this study, the backward difference method was used to solve the transient temperature field, namely, $\beta = 1$. Hence, eq. (16) can be written:

$$([C] + \Delta t [K])T_{n+1} = [C]T_n + \Delta t \{Q\}_{n+1} \quad (17)$$

Results and discussions

In the process of computed simulation, the cooling effect on the surface of the oil groove was considered in determining the convection coefficient. The overall procedure for the thermal analysis is illustrated in fig. 6. To save computing resources and time, only 1/180 of the friction pairs' model was established and the hexahedral structure grid was used to mesh

the friction pairs. To ensure high accuracy of the numerical calculations, a fine mesh was required. The finite element mesh for the steel disc consisted of 14250 elements and 19864 nodes, while that of the friction disc consisted of 29842 elements and 41256 nodes, as shown in fig. 7. The geometric parameters, material properties, and operating conditions used in the analysis are listed in tab. 1.



Figure 7. Finite element model of the friction pairs

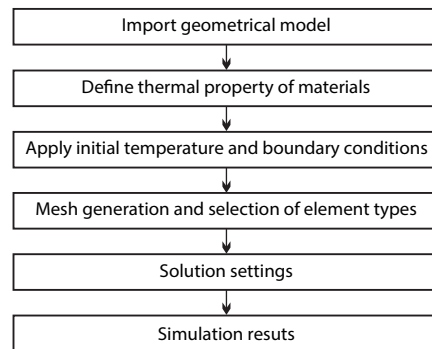


Figure 6. Thermal analysis flowchart

Table 1. The geometric parameters, material properties, and operation conditions

Input data	Value	Input data	Value
Inner diameter of friction pairs [mm]	512	Outer diameter of friction pairs [mm]	664
Thickness of friction lining [mm]	1	Thickness of steel disc and core disc [mm]	1.2
Groove depth [mm]	0.5	Groove width [mm]	1.4
Density of steel disc and core disc [kgm ⁻³]	7800	Specific heat of steel disc and core disc [Jkg ⁻¹ °C ⁻¹]	460
Density of friction lining [kgm ⁻³]	1450	Specific heat of friction lining [Jkg ⁻¹ °C ⁻¹]	1580
Thermal conductivity of steel disc and core disc [Wm ⁻¹ °C ⁻¹]	45	Thermal conductivity of friction lining [Wm ⁻¹ °C ⁻¹]	2.2
Convection coefficient on the inner edge of steel disc [Wm ⁻² °C ⁻¹]	2680	Convection coefficient on the inner edge of friction disc [Wm ⁻² °C ⁻¹]	510
Convection coefficient on the outer edge of steel disc [Wm ⁻² °C ⁻¹]	890	Convection coefficient on the outer edge of friction disc [Wm ⁻² °C ⁻¹]	170
Initial temperature [°C]	30	Ambient oil temperature [°C]	30
Normal pressure [MPa]	1	Frictional coefficient	0.09

Transient temperature of the friction pairs

The maximum and minimum temperatures of the steel disc time history plot are depicted in fig. 8, when the start-up time is 10 seconds. At $t = 8.5$ s, the highest temperature reaches 257.43 °C, which occurs at $r = 0.314$ m, as shown in fig. 9 (this is also illustrated at fig. 10). The heat flux of the contact surface decreased with time, whose influence on the temperature field is significantly less than that of the heat convection at a later stage of the start-up process. Consequently, the temperature stops increasing. During the start-up stage, the temperature difference increases with time ow-

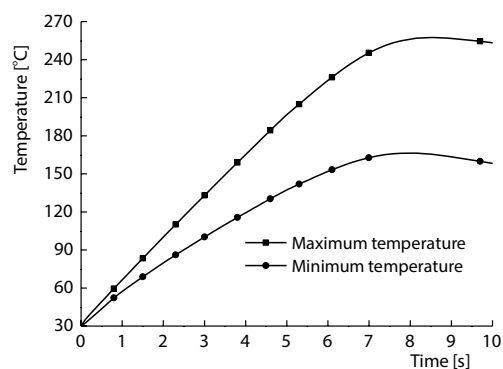


Figure 8. The temperature difference of the steel disc

ing to the continuous heat flux on the friction surface. At the end of the start-up, the temperature difference reaches the maximum value of 95 °C. A significant temperature difference will readily induce a greater thermal stress.

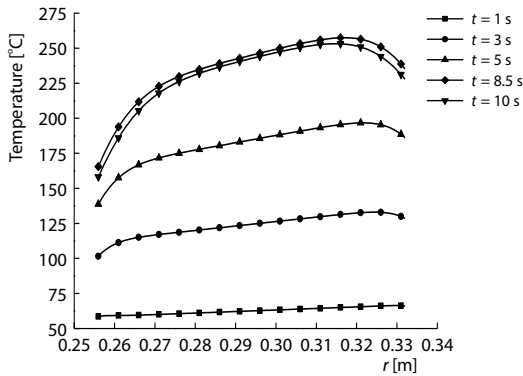


Figure 9. The radial temperatures of the steel disc at the selected time intervals

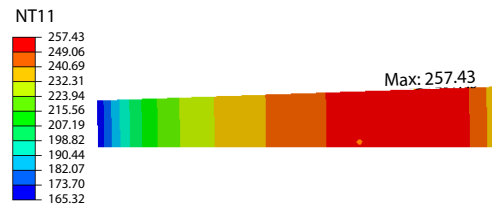


Figure 10. The location of the highest temperature of the steel disc [°C]

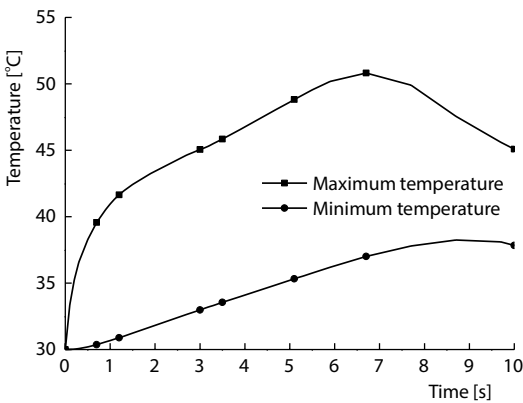


Figure 11. The temperature difference of the friction disc

Figure 12 represents the temperature-time history plot for the friction disc at $r = 0.294$ m. It can be observed that the non-groove temperature increases quickly. At 6.7 seconds, the temperature reaches the maximum value of 47.5 °C at the non-groove, and declines rapidly be-

Figure 9 illustrates the radial temperatures of the steel disc at the selected time intervals. The radial temperature distributions at different moments are approximately similar. The temperature first increases and then declines from the inner radius to the outer radius, which reaches the maximum value at a short distance from the outer edge of the steel disc. Moreover, as time elapsed, it can be observed that the high temperature area comes closer to the center of the steel disc and the radial temperature gradient gradually increases. Basically, this is a sequence of radial heat conduction. Therefore, thermal stress is more likely to be generated. There is intense convection heat transfer with lubricating oil at the two edges of the steel disc. As a result, the temperature at the two edges of the steel disc is lower than that of the middle region. Furthermore, the temperature is lower at the inner radius, in comparison with the temperature at the outer radius, as the heat dissipation at the inner radius is better.

Figure 11 points out the variation of the maximum temperature and minimum temperature of the friction disc during the entire start-up process. The temperature difference increases gradually during the start-up stage. The highest temperature reaches 50.8 °C at $t = 6.7$ s, and occurs at $r = 0.325$ m, as can be seen from fig. 13(d). It is noted that the time and location of the maximum temperature for the friction disc are different from those for the steel disc. This phenomenon occurs because the heat flux is different for the two discs, as can be seen in eq. (13). Additionally, the convection coefficient is unequal. As the heat generated by the friction decreases and the heat exchange with the lubricating oil is obvious, the maximum temperature drops sharply between 6.7 seconds and 10 seconds.

tween 6.7 seconds and 10 seconds. The double arc grooves make more contact with the lubricating oil and reduce their contact with the steel disc concurrently. Therefore, there exists intense convection and little heat flux, which causes the lower temperature in the groove area. Furthermore, owing to the absence of heat flux input, the temperatures of the oil groove and non-groove are consistent at the end of start-up.

The temperature contours of the friction disc at given time moments are shown in fig. 13. The temperature field distribution of the friction disc is extremely similar to that of the steel disc. However, the temperature increase of the friction disc is several times lower than that of the steel disc. The causes of the discrepancy are the significantly different material properties of the steel disc and friction lining. Therefore, deformation occurs frequently on the steel disc. The radial temperature gradient starts to increase with time. Moreover, the temperatures of the central region for each rhombus at the surface of the friction disc are higher than those of the surrounding area, owing to the heat dissipation of the oil groove. The largest temperature is always at the contact surface part, where hot spots may be observed. Generally, from the viewpoint of the failure criterion, the rhombus region is prone to deformation, in comparison to other regions.

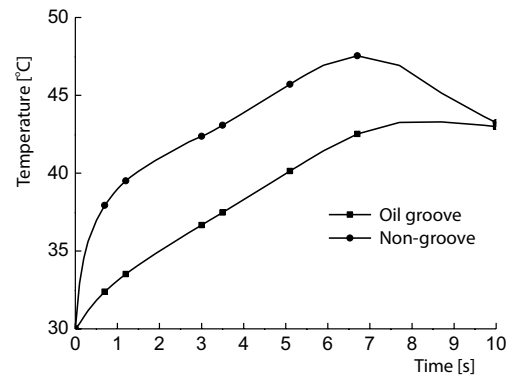


Figure 12. The temperature-time history plot of the friction disc at $r = 0.294$ m

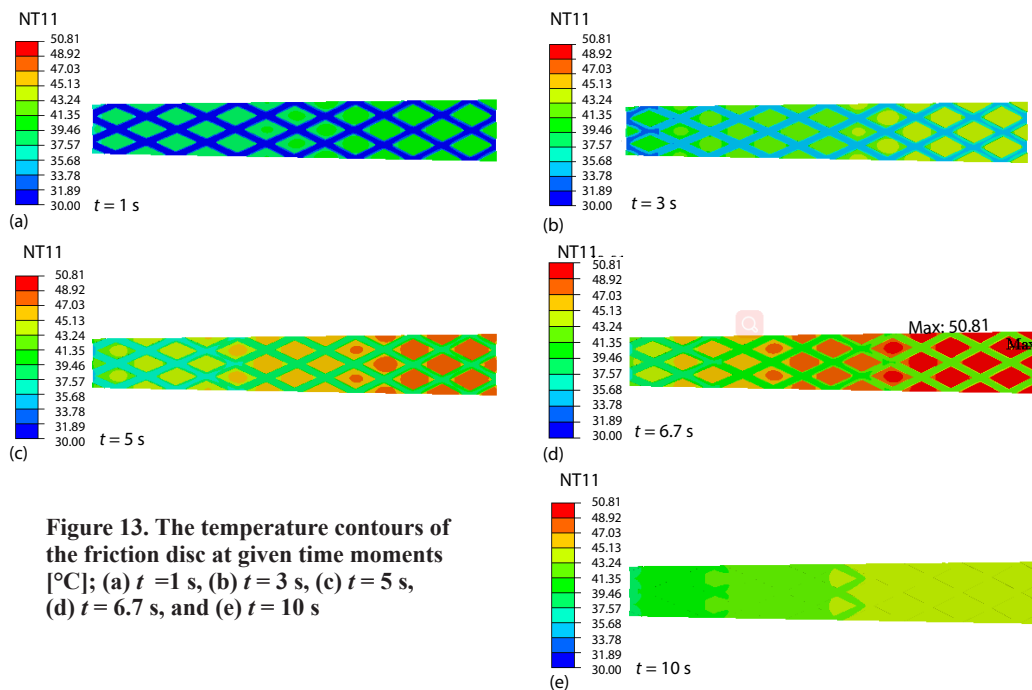


Figure 13. The temperature contours of the friction disc at given time moments [°C]; (a) $t = 1$ s, (b) $t = 3$ s, (c) $t = 5$ s, (d) $t = 6.7$ s, and (e) $t = 10$ s

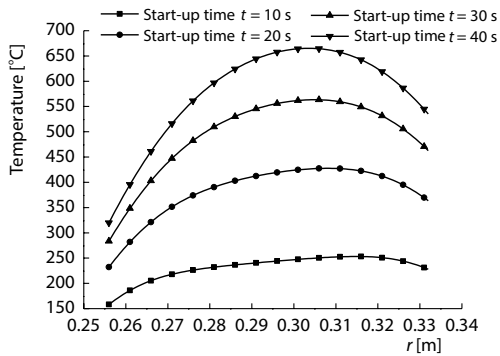


Figure 14. The radial temperatures of the steel disc at the end of start-up

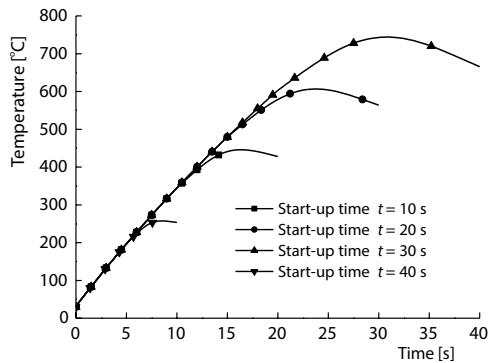


Figure 15. The highest temperature time history plot of the steel disc

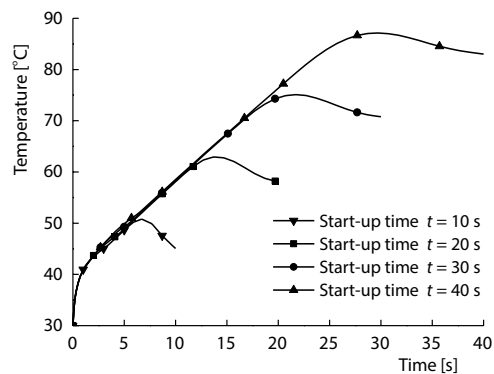


Figure 16. The highest temperature time history plot of the friction disc

Transient temperature of the friction pairs under different start-up times

Figure 14 illustrates the radial temperatures of the steel disc at the end of start-up under different start-up times. The temperature and radial temperature gradient increases gradually as the start-up time increases. This agrees with eq. (10), where the heat flux is proportional to time. Figures 15 and 16 show the results obtained for the maximum temperatures of the steel and friction discs, respectively. It can be observed that the time when the maximum temperature occurs is different for each disc. For instance, when the start-up time is 20 seconds, the maximum temperatures of the steel disc and friction disc are 445.75 °C and 62.92 °C, respectively, at $t = 16.1$ s and $t = 13.7$ s, respectively. Additionally, when the start-up time changes to 40 seconds, the maximum temperatures of the steel disc and friction disc are 744.15 °C and 87.13 °C, respectively, at $t = 30.9$ s and $t = 29.7$ s, respectively. This is caused by an unequal heat flux. Therefore, the start-up time is shown to affect the temperature field of the friction pairs. Nevertheless, the location where the maximum temperature occurs is consistent, as can be seen in figs. 17 and 18. The maximum temperature of the steel disc always appears at $r = 0.314$ m, which is a dangerous area prone to heat failure. However, the maximum temperature of the friction disc occurs at $r = 0.325$ m every time. The simulation results suggest the mutual influence of heat convection and thermal conduction.

Conclusions

In this paper, the temperature field distributions of the double arc groove friction pairs during the entire soft start-up process were analyzed using the finite difference method under start-up times of 10, 20, 30, and 40 seconds. The following conclusions can be drawn from the analysis.

- The temperature and radial temperature gradient of the steel disc are several times those of the friction disc. Therefore, thermal failure may occur in the steel disc.

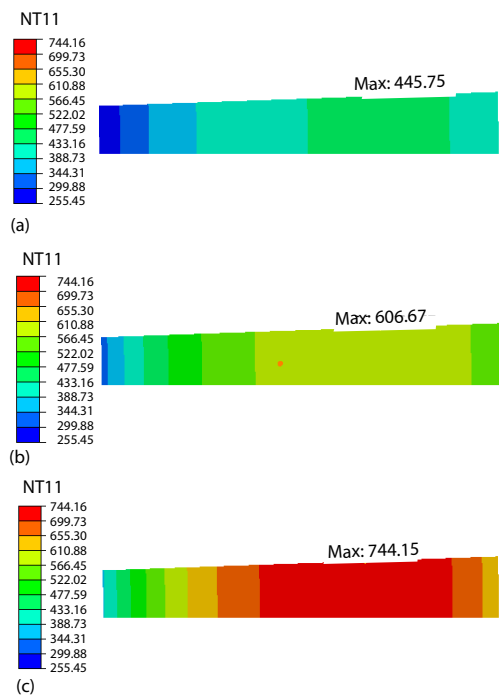


Figure 17. The location of the maximum temperature of the steel disc during the entire start-up process [°C]; (a) start-up time $t = 20$ s, (b) start-up time $t = 30$ s, and (c) start-up time $t = 40$ s

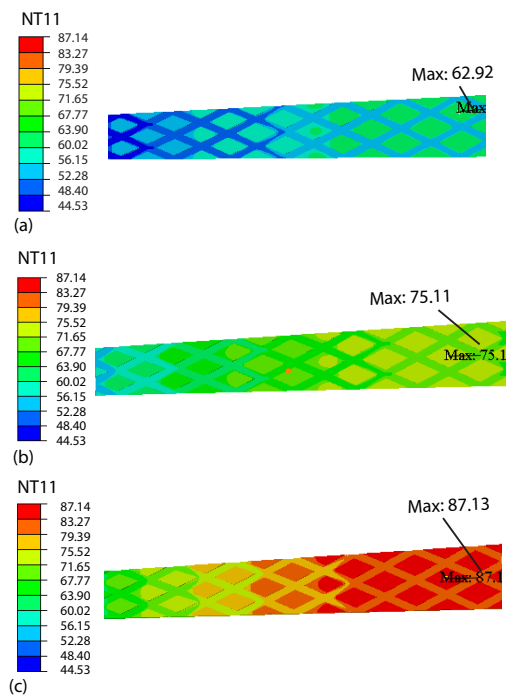


Figure 18. The location of the maximum temperature of the friction disc during the entire start-up process [°C]; (a) start-up time $t = 20$ s, (b) start-up time $t = 30$ s, and (c) start-up time $t = 40$ s

- The double arc groove in the design of the friction disc provides a better cooling system. The rhombus region is prone to deformation, in comparison to other regions.
- The start-up time has a significant impact on the thermal behavior of friction pairs. A larger temperature can be observed when the start-up time is longer. Therefore, a suitable start-up time should be selected according to the actual situation.
- Regardless of how long the start-up time is, the location of the maximum temperature remains unchanged for the steel disc and friction disc, respectively. More attention should be given to these areas.

The calculation results were in good agreement with previous results reported in the literature. This provides a reference and theoretical basis for subsequent thermal stress analysis. Furthermore, it would be interesting to validate the numerical results experimentally.

Acknowledgment

The authors would like to acknowledge the support of the Young Science Research Foundation of Shanxi Province (201601D021066).

Nomenclature

A – thermal conductivity area, [m²]
 c – specific heat capacity, [Jkg⁻¹°C⁻¹]
 $[C]$ – heat capacity matrix, [-]

F – normal force, [N]
 h – oil film thickness, [m]
 k – thermal conductivity, [Wm⁻¹°C⁻¹]

$[K]$	– heat conductivity matrix, [–]
n_j	– speed of output shaft, [rmin ⁻¹]
n_f	– speed of friction disc, [rmin ⁻¹]
n_s	– speed of Sun gear, [Rmin ⁻¹]
q	– heat flux, [Wm ⁻²]
$\{Q\}$	– node heat flux vector, [–]
p	– normal pressure, [MPa]
r	– radius, [m]
t	– time, [s]
T	– temperature, [°C]
T_0	– initial temperature, [°C]
T_a	– ambient oil temperature, [°C]
$\{T\}$	– node temperature vector, [–]
$\{T'\}$	– time derivative of node temperature vector, [–]
z	– thickness, [m]

Greek symbols

α	– convection coefficient [Wm ⁻² C ⁻¹]
γ	– feature parameter of planetary array, [–]
λ	– distribution coefficient of heat flux, [–]
μ	– friction coefficient, [–]
ρ	– density, [kgm ⁻³]
ω	– relative angular velocity, [rads ⁻¹]

Subscripts

c	– core disc
f	– friction lining
s	– steel disc

References

- [1] Wei, C. G., Zhao, J. X., *Technology of Hydro-Viscous Drive* (in Chinese), National Defence Industry Press, Beijing, China, 1996
- [2] Yevtushenko, A. A., et al., Numerical Analysis of Thermal Stresses in Disk Brakes and Clutches (a Review), *Numerical Heat Transfer, Part A, Applications*, 67 (2015), 2, pp. 170-188
- [3] Zagrodzki, P., Truncone, S. A., Generation of Hot Spots in a Wet Multidisk Clutch During Short-Term Engagement, *Wear*, 254 (2003), 3, pp. 474-491
- [4] Marklund, P., Larsson, R., Wet Clutch Friction Characteristics Obtained from Simplified Pin on Disk Test, *Tribology International*, 41 (2008), 9-10, pp. 824-830
- [5] Marklund, P., et al., Thermal Influence on Torque Transfer of Wet Clutches in Limited Slip Differential Applications, *Tribology International*, 40 (2007), 5, pp. 876-884
- [6] Hu, J. B., et al., A Uniform Cross-Speed Model of End-Face Seal Ring with Spiral Grooves for Wet Clutch, *Tribology International*, 62 (2013), 6, pp. 8-17
- [7] Ji, Z. L., et al., Elastoplastic Finite Element Analysis for Wet Multidisc Brake During Lasting Braking, *Thermal Science*, 19 (2015), 6, pp. 2205-2217
- [8] Adamowicz, A., Grzes, P., Analysis of Disc Brake Temperature Distribution During Single Braking under Non-Axisymmetric Load, *Applied Thermal Engineering*, 31 (2011), 6-7, pp. 1003-1012
- [9] Adamowicz, A., Grzes, P., Influence of Convective Cooling on a Disc Brake Temperature Distribution During Repetitive Braking, *Applied Thermal Engineering*, 31 (2011), 14-15, pp. 2177-2185
- [10] Adamowicz, A., Grzes, P., Three-Dimensional FE Model for Calculation of Temperature of a Thermosensitive Disc, *Applied Thermal Engineering*, 50 (2013), 1, pp. 572-581
- [11] Cui, H. W., Research on the Torque Characteristic of Friction Pairs in Hydro-Viscous Clutch (in Chinese), Ph. D. thesis, Beijing Institute of Technology, Beijing, China, 2014
- [12] Cui, H. W., et al., Study on Fluid Torque by Shear Stress of Double Arc Oil Groove Friction Pairs in Hydro-Viscous Drive (in Chinese), *Journal of Chongqing University*, 39 (2016), 5, pp. 1-9
- [13] Xie, F. W., et al., Numerical Simulation Research on Effect of Oil Groove Forms on Thermal Behavior of Friction Pair in Hydro-Viscous Clutch, *Industrial Lubrication and Tribology*, 68 (2016), 2, pp. 287-298
- [14] Cui, J. Z., et al., Numerical Investigation on Transient Thermal Behavior of Multidisk Friction Pairs in Hydro-Viscous Drive, *Applied Thermal Engineering*, 67 (2014), 1, pp. 409-422
- [15] Yevtushenko, A. A., et al., Three-Dimensional FE Model for the Calculation of Temperature of a Disc Brake at Temperature-Dependent Coefficients of Friction, *International Communications in Heat and Mass Transfer*, 42 (2013), Mar., pp. 18-24
- [16] Belhocine, A., Numerical Investigation of a Three-Dimensional Disc-Pad Model with and without Thermal Effects, *Thermal Science*, 19 (2015), 6, pp. 2195-2204
- [17] Belhocine, A., FE Prediction of Thermal Performance and Stresses in an Automotive Disc Brake System, *International Journal of Advanced Manufacturing Technology*, 89 (2016), 9, pp. 3563-3578
- [18] Belhocine, A., Wan Omar, W. Z., Three-Dimensional Finite Element Modeling and Analysis of the Mechanical Behavior of Dry Contact Slipping Between the Disc and the Brake Pads, *International Journal of Advanced Manufacturing Technology*, 88 (2016), 1, pp. 1035-1051

- [19] Belhocine, A., Bouchetara, M., Thermo-Mechanical Behavior of Dry Contacts in Disc Brake Rotor with a Grey Cast Iron Composition, *Thermal Science*, 17 (2013), 2, pp. 599-609
- [20] Adamowicz, A., Axisymmetric FE Model to Analysis of Thermal Stresses in a Brake Disk, *Journal of Theoretical and Applied Mechanics*, 53 (2015), 2, pp. 357-370
- [21] Hsu, T., *The Finite Element Method in Thermomechanics*, Allen & Unwin, Crows Nest, Australia, 1986